JACS
JOURNAL OF THE AMERICAN CHEMICAL SOCIETY
pubs.acs.org/JACS
Article

Chemically Separable Co(II) Spin-State Isomers

Amelia M. Wheaton, Jill A. Chipman, Rebecca K. Walde, Heike Hofstetter, and John F. Berry*

Cite This: J. Am. Chem. Soc. 2024, 146, 26926−26935
Read Online
ACCESS | Metrics & More | Article Recommendations | Supporting Information

ABSTRACT: The phenomenon of spin crossover involves coordination complexes with switchable spin states. This spin state change is accompanied by significant geometric changes such that low and high spin forms of a complex are distinct isomers that exist in equilibrium with one another. Typically, spin-state isomers interconvert rapidly and are similar enough in polarity to prevent their independent separation and isolation. We report here the first example, to our knowledge, of cobalt(II) spin-state isomers that can be physically separated. The reaction of $Mo_2(dpa)_4$ (dpa = 2,2′-dipyridylamide) with $CoBr_2$ produces a mixture of two heterometallic compounds with a linear, metal−metal-bonded Mo≡Mo−Co chain. The complexes, SC-$[BrMo_2(dpa)_4Co]Br$ (SC-**2**) and HS-$[BrMo_2(dpa)_4CoBr]$ (HS-**2**), have identical compositions ($Mo_2Co(dpa)_4Br_2$) but different ground spin states and coordination geometries of the Co(II) ion. In the solid state, SC-**2** undergoes incomplete spin crossover from an $S = 1/2$ state to an $S = 3/2$ state, and HS-**2** has a high spin, $S = 3/2$, ground state, as confirmed by SQUID magnetometry and EPR spectroscopy. Crystallographic analyses of SC-**2** and HS-**2** show that SC-**2** has an elongated Co−Br distance relative to HS-**2** and is best described as the salt $[BrMo_2(dpa)_4Co]Br$. This limits SC-**2**'s solubility in nonpolar solvents and allows for the physical separation of the two isomers. Solution studies of SC-**2** and HS-**2** indicate that SC-**2** and HS-**2** interconvert slowly relative to the NMR time scale. Additional solution-state EPR and UV−vis absorption measurements demonstrate that the choice of solvent polarity determines the predominant isomer present in solution.

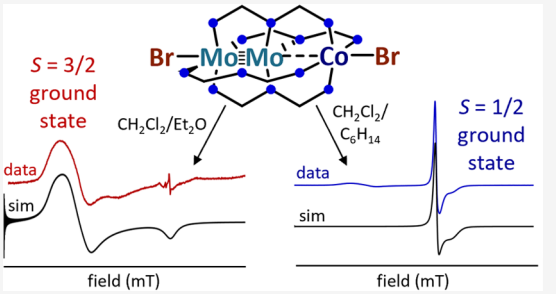

INTRODUCTION

In transition-metal coordination compounds, the phenomenon of spin crossover occurs when a metal center can change between a low spin and a high spin state. This change in spin state is often accompanied by a change in the physical properties of the metal complex and is applicable to molecular sensors and electronic devices.[1−5] For an idealized octahedral Co(II) complex, two possible ground spin states are possible, as emphasized in the Jabłońsky and Tanabe−Sugano style plots in Figure 1a,b, respectively.[1] A low spin complex, ^2E_g, has the $(t_{2g})^6(e_g^*)^1$ configuration, while a high spin complex, $^4T_{1g}$, has a $(t_{2g})^5(e_g^*)^2$ configuration with an additional electron occupying the metal−ligand antibonding e_g^* orbital set. In principle, a Co(II) complex with t_{2g}−e_g^* splitting, $\Delta \approx 20{,}000$ cm^{-1}, would have degenerate ^2E_g and $^4T_{1g}$ states (blue line in Figure 1b). However, the extra antibonding e_g^* electron causes high spin Co(II) complexes to have significantly longer Co−ligand bond distances than low spin complexes[6] and breaks this degeneracy. This geometric difference between the spin states also causes the horizontal offset of the potential wells shown in Figure 1a and a "forbidden zone" shown in Figure 1b that defines a range of Δ values that are physically prohibited.[7] A spin crossover Co(II) complex will therefore exist as a set of ^2E_g and $^4T_{1g}$ isomers, each with different Co−ligand bond distances and magnetic properties that are in equilibrium with one another.[8]

The energetic difference (ΔG_{SC}) between the enthalpically favored low spin state and the entropically favored high spin state of a spin equilibrium system (eq 1) is a more general concept that is applicable to other mixed-spin systems—beyond those of Co(II) spin crossover complexes—which can be influenced by temperature, pressure, light,[9] applied voltage, and strong magnetic fields.[10]

$$^2E_g \rightleftharpoons {}^4T_{2g};\ \Delta G_{SC} \quad (1)$$

In addition, Holm and co-workers described in detail that ΔG_{SC} is more sensitive to fine changes in the complex structure than to the electronics (pK_a) of thiolate ligands in biologically important $[Fe_4S_4(SR)_4]^{3-}$ (SR = alkyl or *para*-substituted arene thiolates) type clusters.[11] Similarly, Andrews and co-workers found that the coordination of noble gas atoms to matrix-isolated CUO and UO_2 molecules provides enough energy to alter the spin state of the U atom from a singlet to a triplet.[12,13]

Received: June 16, 2024
Revised: August 28, 2024
Accepted: August 29, 2024
Published: September 19, 2024

https://doi.org/10.1021/jacs.4c08097
J. Am. Chem. Soc. 2024, 146, 26926−26935

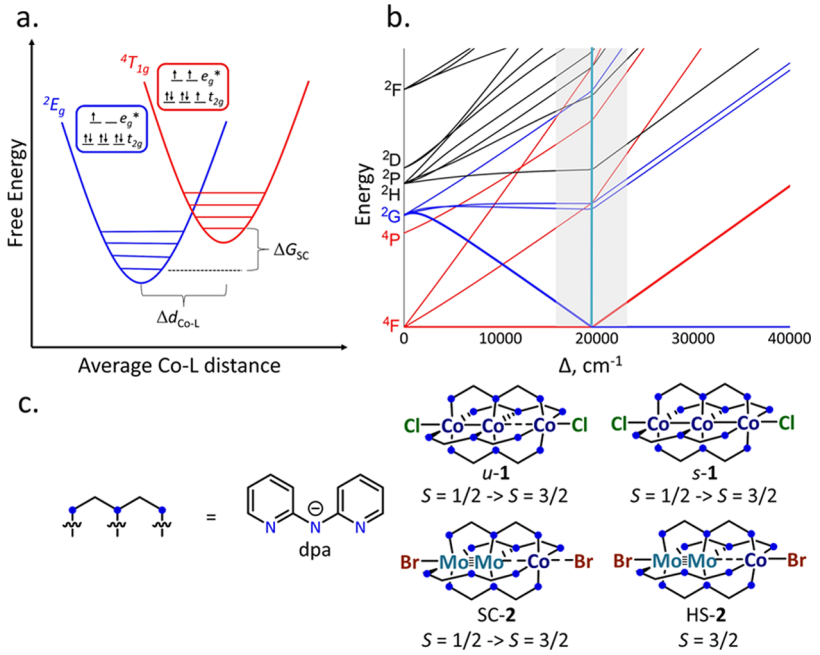

Figure 1. (a) Depiction of the potential energy surfaces for spin equilibrium behavior of an idealized octahedral Co(II) complex where ΔG_{SC} is the energetic difference between the low spin (^2E_g) and high spin ($^4T_{1g}$) states. Electron configurations are provided in the insets. (b) Tanabe−Sugano diagram for Co(II) highlighting the nature of the high spin and low spin ground states, the point of discontinuity that drives spin crossover (blue line), and the forbidden zone of Δ values that are not achievable (gray box). (c, left) structure of the dpa ligand used in this work; (c, right) chemical diagrams depicting the structures and metal−metal bonding behavior of *u*-**1** and *s*-**1** (top) and those of SC-**2** and HS-**2** (bottom).

It comes as no surprise then that crystallization conditions can have a major effect on the properties of spin crossover compounds. For example, increased numbers of crystal defects have been attributed to properties such as gradual spin transitions or incomplete spin crossover.[8] A thoroughly characterized example in which the position of eq 1 is affected by crystallization conditions occurs in the metal−metal bonded, linear tricobalt(II) complex $Co_3(dpa)_4Cl_2$, **1** (Figure 1c), where dpa is the anion of 2,2′-dipyridylamine. Compound **1** crystallizes as two distinct solvatomorphs from a CH_2Cl_2 solution depending on the choice of crystallization antisolvent. The first form crystallizes in an orthorhombic crystal system and contains a Co_3 complex with symmetric Co−Co distances (*s*-**1**) from 20−300 K, whereas the second form crystallizes in a tetragonal crystal system with a Co_3 complex whose set of Co−Co bond distances progress from a symmetric to an unsymmetric arrangement over 20−300 K (*u*-**1**).[14] This difference in the structural features is also represented in the corresponding magnetic data for **1**. Specifically, while *u*-**1** and *s*-**1** possess a common doublet ground state, ^{2}A, with symmetric Co−Co distances, form *u*-**1** undergoes spin crossover to an unsymmetric high spin, ^{4}B state with an onset temperature of ca. 50 K whereas the population of the high spin state for *s*-**1** is not observed until temperatures greater than 200 K.[15]

Clearly, the change in ΔG_{SC} with temperature differs significantly for *u*-**1** and *s*-**1**, as the onset temperature for spin crossover of *u*-**1** is ∼150 K lower than that in *s*-**1**. Additionally, four other crystal structures of **1** were obtained by crystallization from other solvent combinations, and their spin crossover onset temperatures range from 100 to 200 K. Nevertheless, all these compounds possess the same doublet ^{2}A ground state. Thus, while it is possible to modify ΔG_{SC} through different crystallization conditions, this modification generally does not lead to ground state reversal.

True ground spin state reversal is rare but has been observed with drastic changes in geometry within four-coordinate Fe(II)[6,16,17] and Co(II)[18−20] complexes (for example, shifting from a tetrahedral to a square planar geometry either as a result of disruption of a crystal packing effect stabilizing one geometry over another or as a result of dissolution in organic solvents).[21−25] There are even fewer reported examples of five- or six-coordinate complexes. In one instance, Grohmann and co-workers found that crystallization of an octahedral Fe^{II} complex from methanol saturated at room temperature leads to the exclusive formation of a high spin Fe^{II} complex, whereas saturation of the methanol solution at elevated temperatures afforded mixtures of crystals of the high spin form and a second form that undergoes spin crossover from a low to a high spin state.[23] Also, Shores, Yang, and co-workers reported a five-coordinate Co^{II}(ONO) pincer complex that crystallizes with two independent Co complexes in the crystallographic asymmetric unit.[25] One of the symmetry-independent complexes contains a high spin, S = 3/2 ground state at all temperatures, whereas the other undergoes spin crossover from an S = 1/2 to 3/2 ground state. Notably, however, in neither of these cases is a chemical separation of the two isomers reported, nor does this isomerism persist upon dissolution.

More recently, our group has explored electronic and magnetic properties of Co^{II}-based systems using heterometallic Mo≡Mo···Co metal-atom chains that are structurally similar to those of **1**. The homometallic Co−Co−Co and heterometallic Mo≡Mo−Co chains both contain a delocalized three-center-three-electron metal−metal bond stemming from the overlap of the d_{z^2} orbitals of each metal atom in the chain. The introduction of the quadruply bonded metal atom unit results in a shift from a fully covalent metal atom chain to one in

https://doi.org/10.1021/jacs.4c08097
J. Am. Chem. Soc. 2024, 146, 26926−26935

which there is a polar metal−metal interaction between the energetically stabilized orbitals of the Mo_2 and that of the Co heterometal. Thus, this class of complexes provides an opportunity to perturb the spin crossover via metal−metal bonding interactions in addition to the traditional means.

In the case reported here, we observe ground spin state reversal from different crystallization conditions for a pseudo-octahedral Co-based system where the two ground spin state isomers are chemically separable and isolable. The compound of interest is $MoMoCo(dpa)_4Br_2$, **2**, for which syntheses produce two magnetically distinct spin-state isomers: a spin crossover isomer, SC-**2**, which has a low spin ($S = 1/2$) ground state and an isomer with a high spin ($S = 3/2$) ground state, HS-**2**, that can be selectively crystallized from different solvents. Moreover, we demonstrate that it is possible to separate SC-**2** from HS-**2** based on differences in solubility. Crystallographic, magnetic, and EPR measurements of SC-**2** and HS-**2** indicate that the two isomers are chemically and structurally distinct in the solid state. Solution-state electronic absorption, EPR, and 2D ^{1}H NMR measurements indicate that SC-**2** and HS-**2** interconvert slowly in solution and that the position of the spin equilibrium depends on the polarity of the solvent.

RESULTS AND DISCUSSION

Synthesis and Separation. Compound **2** was prepared in an analogous manner to the chloride analog $MoMoCo(dpa)_4Cl_2$, **3** (Scheme 1),[26] via reaction of

Scheme 1. Synthetic Route Used To Access Mixtures of SC-2 and HS-2

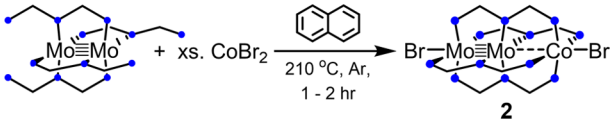

$Mo_2(dpa)_4$ with $CoBr_2$ with molten naphthalene as the reaction "solvent". Initial spectroscopic and magnetic characterization of the dark black crystals isolated from these preparations suggested that despite conforming to the molecular formula of $MoMoCo(dpa)_4Br_2$, the product contained a mixture of paramagnetic products. This surprising result led us to explore methods for chemically separating the paramagnetic species.

We found that a three-step workup of the reaction mixture allowed us to separate the isomers. First, the molten naphthalene reaction mixture is cooled to room temperature, and the naphthalene is removed with multiple hexane washes. This procedure is then followed by multiple washes with $PhCH_3$ that affords a dark orange solution and a remaining black solid. Evaporation of the $PhCH_3$ solution to dryness followed by extraction into CH_2Cl_2 and layering with Et_2O affords crystals of HS-**2**. In turn, SC-**2** was extracted from the $PhCH_3$-washed dark solid with CH_2Cl_2, providing a dark green solution that is layered with hexanes to afford SC-**2** in modest yields. This separation works because SC-**2** is rigorously insoluble in $PhCH_3$ while HS-**2** is slightly soluble. However, the yields of HS-**2** were limited by its low solubility in $PhCH_3$.

Noting that both isomers crystallize from CH_2Cl_2 solution, albeit from different antisolvent mixtures (Et_2O in the case of HS-**2** and hexanes in the case of SC-**2**) we also investigated if we could, by choice of solvents used in crystallization, selectively crystallize HS-**2** directly from the reaction product without the need for an extraction with $PhCH_3$. Extraction of the crude reaction product after hexane washes into CH_2Cl_2 provided a dark brown-green solution which, when layered with Et_2O, provided exclusively crystals of HS-**2** as determined by unit cell measurements of several crystals from the reaction mixture in modest yields. Recrystallization of this material from THF/Et_2O likewise provided only crystals of HS-**2**. In contrast, the recrystallization of crystals of HS-**2** from CH_2Cl_2 and hexanes provided low-quality crystals of SC-**2** and a small amount of dark amorphous material that could not be interrogated crystallographically. While it is possible that the amorphous material consists of uncrystallized SC-**2**, we cannot exclude the possibility that it contains some amount of HS-**2**. Importantly, these experiments demonstrated to us that while the isomer composition of crystals of **2** could be controlled in the solid state, solutions of **2** in CH_2Cl_2 undergo isomerization.

Crystallography. Although SC-**2** and HS-**2** crystallize in different space groups ($C2/c$ and $P2_1/c$, respectively) and with different solvents of crystallization (CH_2Cl_2 and Et_2O, respectively), the heterometallic molecules are identical in composition (Figure 2). In addition to these structures, which

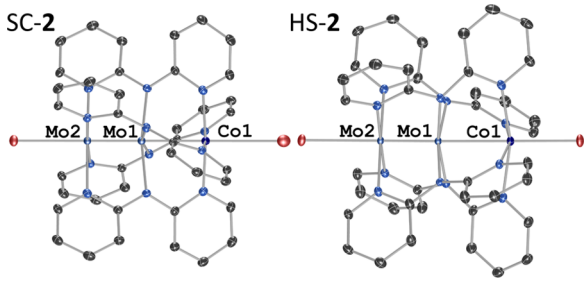

Figure 2. Molecular drawings of SC-**2** (left) and HS-**2** (right) at 100 K shown with selected atom labels and 50% probability ellipsoids. All H atoms, solvent molecules, and minor disorder components have been omitted for clarity. Additional molecular drawings of the crystallographic data discussed in this work are provided in the Supporting Information.

were measured at 100 K, we collected an additional data set for SC-**2** at 295 K (SC-**2**@295) to probe the spin crossover structurally. These structural parameters are listed in Table 1. The table also includes the structural parameters for $Mo_2Co(dpa)_4Cl_2$, **3**, which has a Co center with a high spin, $S = 3/2$ ground state, and does not undergo spin crossover. It is somewhat surprising that changing from Cl ligands to the weaker-field Br ligands changes the spin state energetics in such a way that it can favor a low spin state.

While at first glance the structures of HS-**2** and SC-**2** appear remarkably similar, a closer inspection of each structure's geometric parameters indicates that there are substantial differences in the electronics of the Co^{2+} ion in each structure. For example, the Co−N distances for SC-**2** (1.98 Å) are contracted by ca. 0.13 and 0.20 Å in comparison to those of SC-**2**@295 (2.12 Å) and HS-**2** (2.18 Å), respectively. This difference indicates the population of the Co^{2+} $d_{x^2-y^2}$ metal−ligand antibonding orbital in the high spin species SC-**2**@295 and HS-**2**, which elongates the M−N bonds.[26−28] We may surmise from these data that the Co^{2+} ion of SC-**2** at 100 K exists in a low spin, $S = 1/2$ ground state, whereas the Co^{2+} ions of HS-**2** (at 100 K) exist in the high spin, $S = 3/2$ state.

https://doi.org/10.1021/jacs.4c08097
J. Am. Chem. Soc. 2024, 146, 26926−26935

Table 1. Selected Crystallographic Bond Distances for 2−3[a]

	SC-**2**·2 CH_2Cl_2, 100 K	SC-**2**·2 CH_2Cl_2, 295 K	HS-**2**·$C_4H_{10}O$[b]	**3**·1.5 CH_2Cl_2[c]
Mo−Mo (Å)	2.0971(7)	2.0989(8)	2.0972(16)	2.1027(5)
Mo−Co (Å)	2.4803(8)	2.6372(11)	2.6284(19)	2.6170(7)
M−N (Å)	1.979[13]	2.116[4]	2.1805[5]	2.1025[11]
Mo_i−N (Å)	2.1077[11]	2.119[4]	2.1315[2]	2.1205[4]
Mo_o−N (Å)	2.2255[8]	2.2205[7]	2.1985[11]	2.2155[9]
Mo−L_{ax}[d] (Å)	2.8522(9)	2.8905(11)	2.8768(13)	2.7200(9)
M−L_{ax}[d] (Å)	3.0230(10)	2.6085(11)	2.5254(15)	2.430(1)

[a]Mo_o = outer Mo; Mo_i = inner Mo atom; L_{ax} = Cl (for **3**) or Br (for **2**). [b]In instances of metal-atom chain disorder, the majority position was used for geometric parameters. [c]From ref 26. [d]The (*x*) notation is used to denote standard uncertainties obtained from a single symmetry-independent distance and the [*x*] notation is used for combined standard uncertainties (i.e., uncertainties averaged over multiple symmetry-independent distances).

Interestingly, the Co−N distances of HS-**2** are ca. 0.07 Å greater than those of SC-**2**@295 even though both structures nominally represent high spin Co(II) species. We can rationalize this observation with the magnetic susceptibility studies described below. Specifically, the spin crossover in SC-**2** is incomplete at room temperature, and thus, the Co−N distances are likely shortened due to unresolved crystallographic disorder with molecules of the low spin species. Of equal importance is that the longer Co−N distance in HS-**2** at 100 K indicates that there is no population of a low spin form of the complex at this temperature. Our interpretation of these results is that that SC-**2** is mostly high spin at room temperature while HS-**2** is a fully high spin species at 100 K.

The metal−metal distances also support this interpretation. The Mo−Co distance for SC-**2** increases by almost 0.15 Å from 100 to 295 K and the Mo−Co distances for HS-**2** and $Mo_2Co(dpa)_4Cl_2$, **3**, are comparable with SC-**2**@295, indicating that SC-**2**@295 is mostly high spin. The shorter Mo−Co distance of 2.48 Å in the low spin form of SC-**2** (100 K) is comparable to the Cr−Co distance of 2.49 Å in the low spin form of the related spin crossover compound $Cr_2Co(dpa)_4Cl_2$, **4**, at 100 K.[26]

In contrast to the shorter Mo−Co distance, the Co−Br distance for SC-**2** at 100 K is extremely long, 3.02 Å. This distance is even longer than the sum of the covalent radii of the Co and Br atoms,[29] but shorter than the sum of their van der Waals radii.[30] In contrast, the Co−Br distances for SC-**2**@295 and HS-**2** (2.61 and 2.53 Å, respectively), are similar to the more typical Co(II)−Br bonds in $Co_3(dpa)_4Br_2$ (2.66 Å).[31] These Co−Br distances provide a rationalization for the chemical separability of the two isomers. Specifically, the crystallographic data suggest that at 100 K SC-**2** is best described as a salt, $[Mo_2Co(dpa)_4Br]^+[Br]^-$, with the low spin Co^{2+} ion adopting a square pyramidal geometry and the Br^- axial "ligand" practically dissociated from the Co^{2+} center. As a result, the low spin form of SC-**2** is insoluble in nonpolar solvents such as $PhCH_3$, which allows for its separation from HS-**2**.

Physical Measurements. The magnetic susceptibility (χ) and reduced magnetization (M) data, as determined from SQUID magnetometry measurements on microcrystalline samples of SC-**2** and HS-**2**, are shown in Figure 3, with fitted

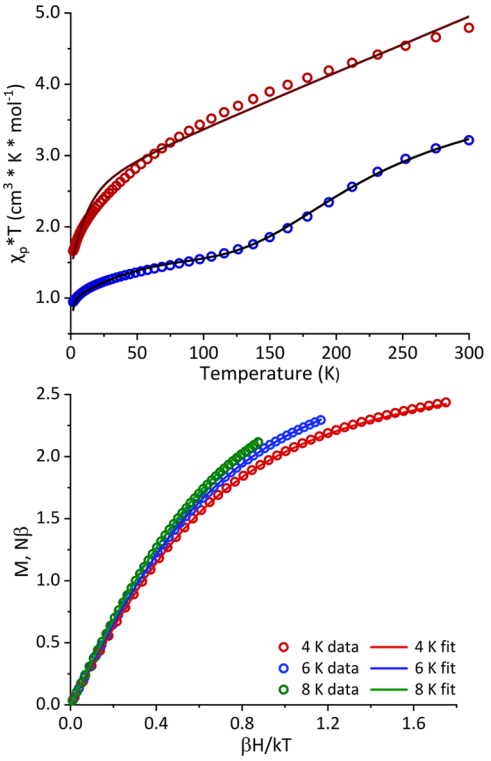

Figure 3. Top: magnetic susceptibility data and models for SC-**2** (blue) and HS-**2** (red). Bottom: reduced magnetization data and fits for HS-**2**.

or simulated parameters given in Table 2. In the fit for HS-**2**, the g values are fixed to the values determined by EPR spectroscopy (vide infra); an alternative fit in which the g values were allowed to be freely refined is given in Figure S9.

Complexes HS-**2** and SC-**2** display remarkably distinct magnetic properties despite their identical chemical composition. The magnetic behavior of HS-**2** is consistent with a single, high spin Co^{2+} ion with large magnetic anisotropy manifested as zero-field splitting. Magnetic susceptibility and reduced magnetization data for HS-**2** were fitted simultaneously, using a nearly axial model for the S = 3/2 Co^{2+} center (E/D = 0.11, consistent with the EPR data) and a positive D of 12 cm^{-1} (Table 2).

In contrast, SC-**2** displays markedly different magnetic behavior, with χT of 0.97 cm^3 mol^{-1} K at 1.8 K, which rises taking on a curvature at ca. 150 K. This sigmoidal behavior of $\chi \cdot T$ vs T is expected for a spin crossover species and is consistent with a spin equilibrium between the S = 1/2 and 3/2 states. It should be noted that the aforementioned $Co_3(dpa)_4X_2$ complexes[14,31−34] and $Cr_2Co(dpa)_4X_2$ with X = Cl or N_3 complexes also contain Co^{2+} ions that undergo S = 1/2 to S = 3/2 spin crossover.[26]

However, the χT value of ca. 1.0 cm^3 K mol^{-1} in the low-temperature regime (<100 K) is above the spin-only χT value expected for an S = 1/2 system (0.375 cm^3 K mol^{-1}). Moreover, the value of $\chi \cdot T$ at the high-temperature limit is well above the spin-only value expected for an S = 3/2 system (1.875 cm^3 K mol^{-1}) but significantly lower than that for HS-**2** in the high-temperature range. Both effects are consistent with

https://doi.org/10.1021/jacs.4c08097
J. Am. Chem. Soc. 2024, 146, 26926−26935

Table 2. SQUID Simulation Parameters for SC-2 and Fit Parameters for HS-2; EPR Simulation Parameters for Powder Samples of SC-2 and HS-2

	SC-2		HS-2		HS-2[c]		SC-2 EPR		HS-2 EPR
g_{LS}, iso[a]	2.18	g_1[a]	2.00	$g_\parallel$	2.40(5)	$g_\parallel$	2.02	g_1	2.0
TIP_{LS}, $cm^3\ mol^{-1}$	0.002	g_2[a]	2.50	$g_\perp$	2.69(3)	$g_\perp$	2.26	g_2	2.5
g_{HS}, $\parallel$[a]	2.00	g_3[a]	2.57	D, cm^{-1}	52.1(8)			g_3	2.57
g_{HS}, $\perp$[a]	2.54	D, cm^{-1}	12.85(2)	TIP, $cm^3\ mol^{-1}$	0.00570(6)			E/D	0.1
D_{HS}, cm^{-1}	31	E, cm^{-1}	1.44(4)	zJ, cm^{-1}	−0.42(1)			A_1 (^{57}Co), MHz	170
TIP_{HS}, $cm^3\ mol^{-1}$	0.003	E/D	0.11	Residual[b]	0.0058			A_2 (^{57}Co), MHz	180
ΔH, kJ mol^{-1}	8	TIP, $cm^3\ mol^{-1}$	0.00777(5)					A_3 (^{57}Co), MHz	0
T_C, K	212	zJ, cm^{-1}	−0.21(3)						
PHS, %	38	Residual[b]	0.0055						
Residual[b]	0.022								

[a]g values are fixed to those determined by EPR spectroscopy. [b]Residual = $[\sum_{i=1}^{points}(M_{exp} - M_{cals})^2][\sum_{i=1}^{points}(\chi_{exp} - \chi_{cals})^2]$ where M_{exp}/M_{calc} = measured/calculated magnetization and χ_{exp}/χ_{calc} = measured/calculated susceptibility. [c]Alternative fit of HS-2 allowing the g values to refine freely.

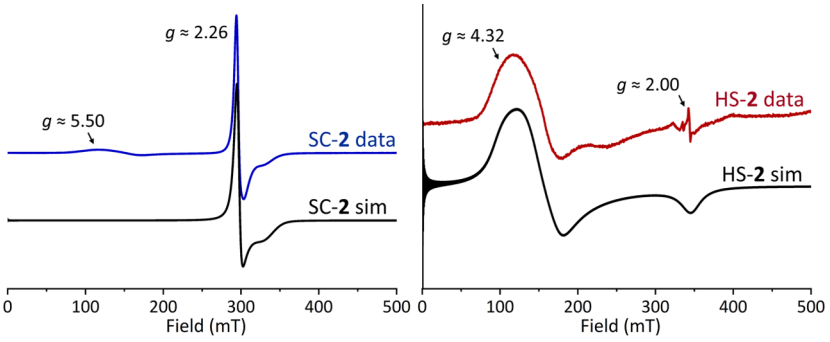

Figure 4. X-band EPR spectra of SC-2 (left) and HS-2 (right) as powder samples at 10 K. The data were simulated by using spin Hamiltonian models for $S = 1/2$ and $S = 3/2$ systems, respectively.

the incomplete spin crossover of the Co^{2+} ion of SC-2, vide infra.

Taken together, these data suggest that samples of SC-2 undergo incomplete spin crossover and that a portion of the Co^{2+} ions remain at high spin at all temperatures. This could either be due to contamination of SC-2 with a small amount of HS-2 or due to an intrinsic property of the structure of SC-2. We simulated the susceptibility data for SC-2 with the Raoult's law spin equilibrium expression[35] below.

$$\chi T = (1 - P_{HS})\frac{F_{HS} - F_{LS}}{1 + \exp[\frac{\Delta H}{R}\cdot(\frac{1}{T} - \frac{1}{T_C})]} + P_{HS}\cdot F_{HS}$$

Here, T_C is the critical temperature (the temperature where there are an equal number of high and low spin molecules), P_{HS} is the portion of the complex that remains high spin at all temperatures, and ΔH is the enthalpy difference between the low and high spin states. F_{HS}/F_{LS} are functions that describe the temperature dependence of the high and low spin states; they depend on the g factors and TIP correction for the high and low spin states. The F_{HS} function also accounts for the zero-field splitting (D) present in the high spin state of SC-2

$$F_{LS} = \left(\frac{g_{LS}^2}{4}\cdot\frac{3}{8}\right) + TIP_{LS}\cdot T$$

$$F_{HS} = \left(\frac{\chi_\parallel + 2\chi_\perp}{3}\right) + TIP_{HS}\cdot T$$

where

$$\chi_\parallel = \frac{3g_{HS,\parallel}^2}{32}\cdot\frac{1 + 9\exp(-2x)}{1 + \exp(-2x)}$$

$$\chi_\perp = \frac{3g_{HS,\perp}^2}{8}\cdot\frac{\left(1 + \frac{3}{4x}\right)\cdot\left(1 - \exp\left(-2x\right)\right)}{1 + \exp(-2x)}$$

and

$$x = D/kT$$

The g values of F_{LS} and F_{HS} were fixed to those obtained from the EPR spectra of SC-2 and HS-2, respectively.

X-band EPR spectra of powder samples of HS-2 and SC-2 at 10 K are shown in Figure 4, and the two isomers again display remarkably distinct features. The spectrum of HS-2 contains a broad, rhombic signal with effective g values of ∼4.32 and ∼2.00. These features are characteristic of a high spin, $S = 3/2$ species with large zero-field splitting ($D > h\nu$). Simulation of the spectrum yields intrinsic g values of 2.0, 2.5, and 2.57, and rhombicity, E/D of 0.1. For SC-2, an axial signal is observed ($g_\parallel = 2.02$, $g_\perp = 2.26$). This signal is similar to that reported for the five-coordinate, square pyramidal, low spin Co^{2+}complex $[Co(dppe)_2(NCCH_3)](BF_4)_2$ ($g_1 = 2.009$, $g_2 = 2.262$, $g_3 = 2.290$),[36] consistent with a $(d_{z^2})^1$ electron configuration for both species. There is also a broad feature at $g \sim 5.50$, likely from residual HS-2.

Remarkably, the combination of magnetic and 10 K EPR data demonstrates that, in the solid state, SC-2 and HS-2 have different ground spin states despite consisting of the same molecular species.

https://doi.org/10.1021/jacs.4c08097
J. Am. Chem. Soc. 2024, 146, 26926−26935

Solution Characteristics. Having now established that SC-**2** and HS-**2** possess distinct ground spin states in the solid state, we sought to explore whether the two species retain their spin state identities in solution. For context, spin state changes in coordination complexes typically occur on the time scale of nanoseconds,[37] although distinct spin state isomers have been observed occasionally in solution. For example, the $[Fe_4S_4(SR)_4]^{3-}$ clusters, with diverse ground spin states in the solid state, all contain a mixture of $S = 1/2$ and $S = 3/2$ ground state species when frozen in DMF solutions as determined by EPR (7 K) and Mössbauer spectroscopies.[11] However, it was found that the homometallic Co_3 complexes *s*-**1** and *u*-**1** interconvert quickly in solution such that only one, symmetric, species is observable by NMR spectroscopy.[14,32,33,38] In the case of SC-**2** and HS-**2**, the difference in solubilities of the two species and their separability suggest that interconversion may be slow. Furthermore, the selective solubility of HS-**2** indicated to us that we could use solutions of HS-**2** in nonpolar solvents to measure the spectroscopic properties of HS-**2** independently from those of SC-**2**. To perform operational tests of these ideas, we used three different solution samples of **2**. First, we studied solutions of SC-**2** and HS-**2** in CH_2Cl_2 (a solvent in which both isomers are soluble) to test for interconversion between the two isomers. We then compared the solutions of SC-**2** and HS-**2** in CH_2Cl_2 to that of a third sample, HS-**2** in $PhCH_3$ (a solvent that only HS-**2** is soluble in), to determine what similarities and differences there were between the three solutions.

We chose three methods to study the solution behavior of SC-**2** and HS-**2** in CH_2Cl_2 and HS-**2** in $PhCH_3$: electronic absorption spectroscopy, EPR spectroscopy, and NMR spectroscopy. The results of those measurements are discussed in this order below.

One of the first indications that the chemical separation of SC-**2** and HS-**2** was viable arose from the qualitative observation that solutions of SC-**2** and HS-**2** have different colors in CH_2Cl_2 (dark brown-green) and $PhCH_3$ (dark orange). Electronic absorption spectra of SC-**2** in CH_2Cl_2, HS-**2** in CH_2Cl_2, and HS-**2** in $PhCH_3$ are shown in Figure 5 with the λ_{max} for each feature (labeled A–E) provided in Table S3. The different colors of the compounds in CH_2Cl_2 and $PhCH_3$ are substantiated by the strikingly different spectral features in these solvents. Both SC-**2** and HS-**2** in CH_2Cl_2 have a similar overall absorption profile, with major absorption maxima at ~480 and ~580 nm (bands B and C in Figure 5) with a shoulder at ~660 nm attributable to the Mo≡Mo $\delta-\delta^*$ transition (band D in Figure 5).

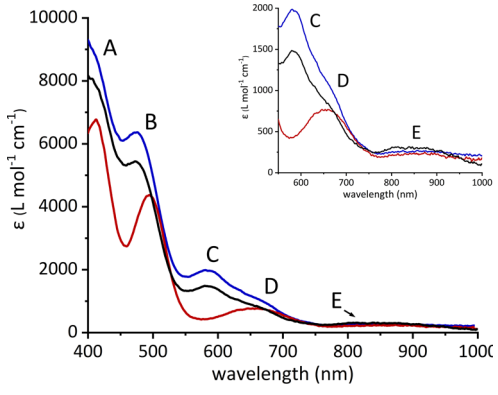

Figure 5. Electronic absorption spectra of SC-**2** (blue) and HS-**2** in CH_2Cl_2 (black) and of HS-**2** in $PhCH_3$ (red). The inset is an expansion of the low-energy features.

In contrast, HS-**2** in $PhCH_3$ notably lacks band C; furthermore bands B and D are shifted bathochromically by ~10 nm (ca. 590 cm^{-1}) as compared to the CH_2Cl_2 solution spectra. These spectra indicate that the compounds SC-**2** and HS-**2** behave similarly in CH_2Cl_2 solution, likely containing a mixture of low and high spin Co(II) species. In $PhCH_3$, however, only one species is present.

These conclusions are further supported by the EPR spectra shown in Figure 6. Notably, the EPR spectra of SC-**2** and HS-**2**

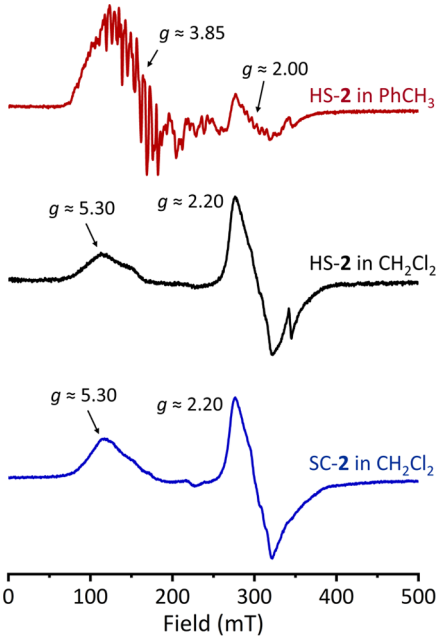

Figure 6. X-band EPR spectra at 10 K of HS-**2** in $PhCH_3$ (top, red), HS-**2** in CH_2Cl_2 (middle, black), and SC-**2** in CH_2Cl_2 (bottom, blue).

in CH_2Cl_2 are extremely similar. In each spectrum, two signals are observed corresponding to distinct spin systems, which can be assigned by referring to the solid-state EPR spectra shown in Figure 4. The first spin system shows a rhombic signal centered at ca. $g = 2.20$ and a slight stair-step-like pattern that is consistent with unresolved hyperfine of the $I = 7/2$ ^{59}Co nucleus. This feature is comparable to that observed for SC-**2** in the solid state but is more broad, likely due to multiple conformations being accessible in solution. This feature is therefore assignable to an $S = 1/2$ low spin Co(II) species present in samples of both SC-**2** and HS-**2** in CH_2Cl_2 at 10 K. Both EPR spectra also contain a broad feature centered at g ~ 5.30, which is reminiscent of the spectrum of HS-**2** in the solid state. We therefore assign this signal to an $S = 3/2$ high spin Co(II) species that is present in both SC-**2** and HS-**2** in CH_2Cl_2 solution.

The EPR spectrum of HS-**2** in $PhCH_3$ is dramatically different from that of HS-**2** in CH_2Cl_2. The main signal is a rhombic feature with effective g values of ~3.85 and ~2.00 with extensive hyperfine splitting. The g values suggest an $S = 3/2$ high spin Co(II) species with large zero-field splitting, similar to what was found for HS-**2** in the solid state.

These EPR spectra demonstrate that both low and high spin Co(II) species are present upon dissolution of either SC-**2** or

https://doi.org/10.1021/jacs.4c08097
J. Am. Chem. Soc. 2024, 146, 26926–26935

HS-**2** in CH_2Cl_2. Additionally, the equilibrium amounts of low spin and high spin Co(II) species in solution are similar regardless of whether the SC-**2** or HS-**2** compound is dissolved, suggesting that the two spin state isomers interconvert in solution. However, the equilibrium distribution between the low and high spin isomers is trapped by freezing the samples which are unable to interconvert in the "solid-state" frozen solution on the EPR time scale at 10 K. The equilibrium distribution can also be forced toward HS-**2** by the use of a nonpolar solvent ($PhCH_3$), which likely stabilizes a less ionic Co−Br interaction.

Taken together, the electronic absorption and solution EPR measurements suggest that, in CH_2Cl_2 solution, SC-**2** or HS-**2** display an identical equilibrium mixture of low spin Co(II) and high spin Co(II) isomers whereas only the high spin Co(II) isomer is observed in $PhCH_3$ solution. These observations are also corroborated by the room-temperature solution ^{1}H NMR spectra of SC-**2** and HS-**2** in CD_2Cl_2 and HS-**2** in toluene-d^8. While SC-**2** and HS-**2** are paramagnetic, their NMR spectra display an array of sharp signals due to pyridyl hydrogen atoms that are shifted out of the diamagnetic range as shown in Figure 7 (see Figure S16 for the diamagnetic region). There

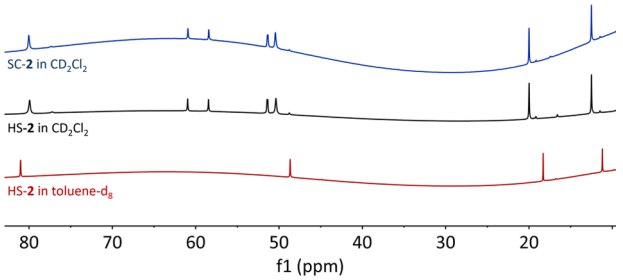

Figure 7. Room-temperature ^{1}H NMR spectra of SC-**2** (top, blue) and HS-**2** (middle, black) in CD_2Cl_2, as well as the ^{1}H NMR spectrum of HS-**2** in toluene-d^8 (bottom, red).

are several notable features that are worth discussing. First, the NMR spectra of SC-**2** and HS-**2** in CD_2Cl_2 are almost identical, with both spectra including the magnetically shifted resonances at positions given in Table 3 (see Figures S8−S13 for full NMR spectra). The molecular structure of $Mo_2Co(dpa)_4Br_2$, with idealized C_4 symmetry, should give rise to eight unique hydrogen atom resonances but there are at least ten signals observed in the ^{1}H NMR spectra of SC-**2** and HS-**2** in CD_2Cl_2. Thus, these spectra suggest that more than one species is present in a CD_2Cl_2 solution. Precise integration of the spectral peaks is difficult due to paramagnetic broadening, especially for the signals outside of the range shown in Figure 7. However, the signals in Figure 7 for SC-**2** and HS-**2** in CD_2Cl_2 integrate to roughly equal intensity, suggesting that, if the solution contains both low spin Co(II) and high spin Co(II) isomers, they are present in a ∼1:1 ratio.

Importantly, the ^{1}H NMR spectrum of HS-**2** in toluene-d^8 contains only five specific signals, given in Table 3, with roughly equal integrated intensities. The fact that the toluene-d^8 spectrum contains substantially fewer paramagnetically shifted signals than the spectra in CD_2Cl_2, taken together with the results of the absorption and EPR characterization of solutions of **2** in $PhCH_3$, suggests that only HS-**2** is present in toluene-d^8 solutions. The toluene-d^8 NMR data may therefore be used as a reference spectrum to facilitate signal assignments in CD_2Cl_2 solutions.

Armed with this information, we sought to acquire 2D COSY (^{1}H−^{1}H) NMR spectra of SC-**2** in CD_2Cl_2 and HS-**2** in toluene-d^8 at 258 K in an attempt to fully assign the observable NMR signals. Using protocols outlined by McConnell and co-workers,[39] we obtained remarkably sharp COSY data for these solutions despite the paramagnetism of the compounds. The COSY NMR spectrum of HS-**2** in toluene-d^8 (Figure 8, right, and Table 4) displays four unique visible cross peaks that correspond to two ring systems. The first ring system we assign to the dpa pyridyl ring is bound to the paramagnetic Co(II) center and contains the coupled resonances observed at 93.59, 57.41, and 21.62 ppm. While the resonance at 121 ppm does not show visible correlations, we also assign it to this ring system due to its strong paramagnetic shift. The second ring system then corresponds to the pyridyl ring bound to the diamagnetic Mo_2 unit and contains peaks at 12.82 ppm, 6.85 ppm, 1.64 ppm, and likely −2.31 ppm, though again the last peak could not be assigned with certainty due to a lack of correlations.

Deconvolution of the COSY spectrum of SC-**2** in CD_2Cl_2 at 258 K (Figure 8, left, and Table 4) is relatively straightforward with the assistance of the assignments of the COSY spectrum in toluene-d^8. Comparison of the two spectra accounting for the differing solvents allow us to assign the resonances at 117, 96.17, 57.51, and 22.5 ppm to the Co-pyridyl ring system within HS-**2** and those at 14.04, 7.6, 1.6, and −3.72 ppm to the Mo_2-pyridyl ring system within HS-**2**. The remaining correlations can then be assigned to the low spin species as follows: the Co-pyridyl ring system consists of the resonances at 87.93, 56.53, and 22.94 ppm. The Mo_2-pyridyl ring system consists of the resonances at 9.73, 6.18, and 1.27 ppm.

The observation of signals from both low spin and high spin species in CD_2Cl_2 suggests that, at room temperature, the spin state isomers interconvert slowly relative to the NMR time scale. In order to substantiate this hypothesis and motivated by the sharp COSY signals, we performed NOSEY (Figures S23−S27) measurements on a CD_2Cl_2 solution of SC-**2** at 258 K The NOESY spectra of SC-**2** in CD_2Cl_2 at 258 K are again quite sharp (Figures S23−S27). We observe one major cross peak that connects the 96.17 and 87.93 ppm resonances. Notably, each of the resonances that contribute to this cross peak was assigned to different spin states of the molecule in solution. This result, in conjunction with the fact that the cross peak is of the same sign as the diagonal, demonstrates that there is a chemical exchange in solution between low spin and high spin forms of SC-**2** that is slow relative to the NMR time scale, though further quantification of the interconversion rate was prohibited due to paramagnetic broadening of the signal. The fact that the isomers are slow to interconvert, along with

Table 3. ^{1}H NMR Resonances for 2 in Room-Temperature CD_2Cl_2 and Toluene-d^8

solvent	^{1}H resonances, ppm (referenced to TMS)									
CD_2Cl_2	106.4	83.2	79.9	60.9	58.4	51.4	50.4	20.0	12.5	−1.0
toluene-d^8	106.3	81.0	48.6	18.3	11.2					

https://doi.org/10.1021/jacs.4c08097
J. Am. Chem. Soc. 2024, 146, 26926−26935

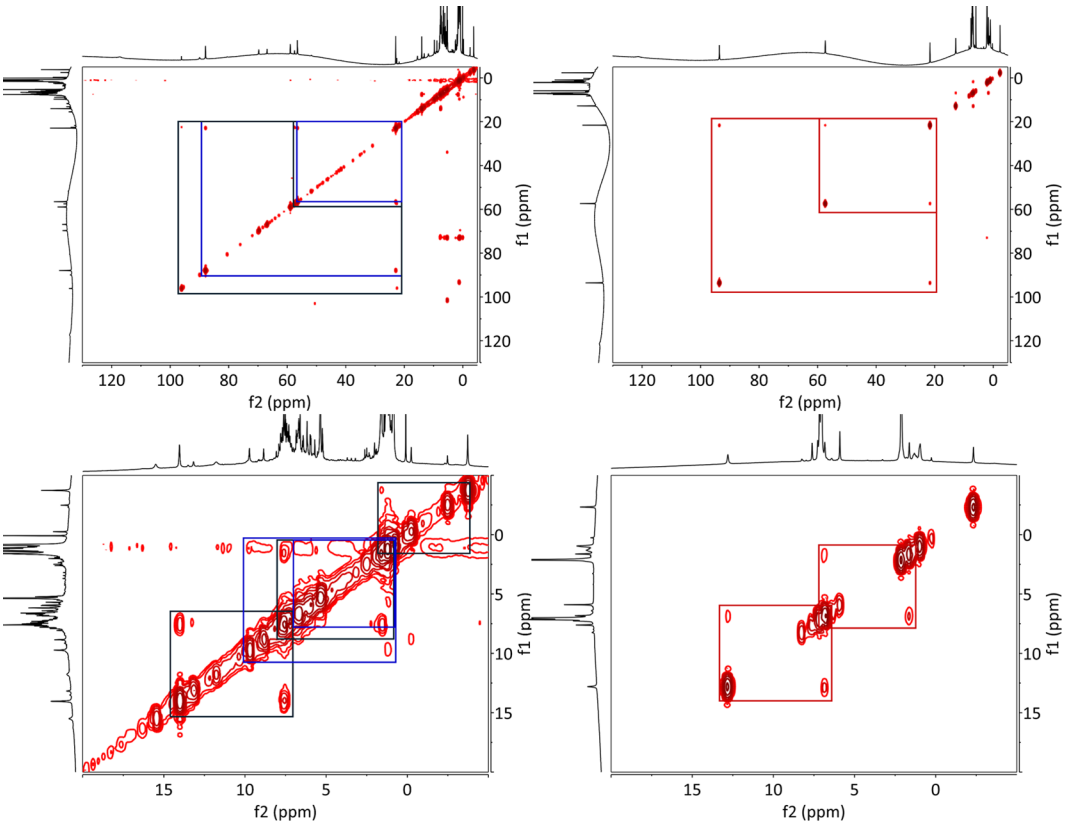

Figure 8. $^{1}H-^{1}H$ COSY NMR spectra of SC-**2** in CD_2Cl_2 (left) and of HS-**2** in toluene-d^8 (right) at 258 K. The upper spectra are shown from 130 to −5 ppm, and the lower spectra are shown from 20 to −5 ppm. The boxes are used to highlight the correlations between resonances corresponding to the high (black) and low (blue) spin species in CD_2Cl_2 and the single (high spin) species in toluene-d^8 (red). The cross-peaks corresponding to the high spin species in CD_2Cl_2 are as follows: [96.2, 22.6], [57.51, 22.6], [14.0, 7.60], [7.60, 1.59], [1.59, −3.72]. For the low spin species in CD_2Cl_2, the cross-peaks are [87.9, 22.9], [56.5, 22.9], [9.73, 1.27], and [6.18, 1.27]. The cross-peaks in toluene-d^8 (all assigned to HS-**2**) are [93.6, 21.6], [57.41, 21.6], [12.8, 6.85], and [6.85, 1.64].

Table 4. Assignments of Resonances in the ^{1}H Spectra of 2 in Toluene-d^8 and CD_2Cl_2 Solutions at 258 K

	Co-pyridyl ring resonances, ppm				Mo_2-pyridyl ring resonances, ppm			
toluene-d^8 (HS-**2**)	121	93.6	57.4	21.6	12.8	6.85	1.64	−2.31
CD_2Cl_2 (high spin)	117	96.2	57.5	22.6	14.0	7.60	1.59	−3.72
CD_2Cl_2 (low spin)	87.9	56.5	22.9		9.73	6.18	1.27	

the structural differences that give rise to the different solubilities of the two isomers, underpins our ability to chemically separate and isolate these spin-state isomers.

CONCLUSIONS

We describe here the synthesis of chemically distinct forms of $Mo_2Co(dpa)_4Br_2$ (SC-**2** and HS-**2**) heterometallic extended metal atom chain complexes that differ in the ground spin state of the Co(II) ion and that are prepared from the same molten naphthalene mixture. A combination of crystallographic analysis, SQUID magnetometry measurements, and solid-state EPR spectroscopy demonstrates that while SC-**2** supports a Co(II) ion with an $S = 1/2$ ground state that undergoes incomplete spin crossover, HS-**2** supports a Co(II) ion with an $S = 3/2$ ground state. Solution studies using electronic absorption, EPR, and 1D and 2D ^{1}H NMR spectroscopy demonstrate that while SC-**2** and HS-**2** interconvert slowly to a mixture of high and low spin Co(II) species in CH_2Cl_2 solutions, solutions of HS-**2** in $PhCH_3$ maintain the presence of only a high spin, $S = 3/2$ Co(II) ion. These solid-state and solution studies allow us to rationalize the persistent chemical separability of SC-**2** and HS-**2** as arising from both structural differences between the two isomers' Co−Br axial sites and the slow interconversion of SC-**2** and HS-**2** in CH_2Cl_2 solution.

ASSOCIATED CONTENT

Supporting Information

The Supporting Information is available free of charge at https://pubs.acs.org/doi/10.1021/jacs.4c08097.

Synthetic methods and experimental details of physical measurement techniques, crystallographic refinement details and additional figures, alternative models of HS-**2** magnetic data, and additional ^{1}H and 2D NMR spectra (PDF)

Accession Codes

CCDC 2339170, 2339180, and 2339181 contain the supplementary crystallographic data for this paper. These data can be obtained free of charge via www.ccdc.cam.ac.uk/data_request/cif, or by emailing data_request@ccdc.cam.ac.uk, or by contacting The Cambridge Crystallographic Data

https://doi.org/10.1021/jacs.4c08097
J. Am. Chem. Soc. 2024, 146, 26926−26935

Centre, 12 Union Road, Cambridge CB2 1EZ, UK; fax: + 44 1223 336033.

AUTHOR INFORMATION

Corresponding Author

John F. Berry − *Department of Chemistry, University of Wisconsin−Madison, Madison, Wisconsin 53706, United States;* orcid.org/0000-0002-6805-0640; Email: berry@chem.wisc.edu

Authors

Amelia M. Wheaton − *Department of Chemistry, University of Wisconsin−Madison, Madison, Wisconsin 53706, United States;* orcid.org/0000-0002-7743-9922

Jill A. Chipman − *Department of Chemistry, University of Wisconsin−Madison, Madison, Wisconsin 53706, United States;* orcid.org/0000-0002-3243-8766

Rebecca K. Walde − *Department of Chemistry, University of Wisconsin−Madison, Madison, Wisconsin 53706, United States;* orcid.org/0000-0002-3320-2085

Heike Hofstetter − *Department of Chemistry, University of Wisconsin−Madison, Madison, Wisconsin 53706, United States;* orcid.org/0000-0003-4501-4206

Complete contact information is available at: https://pubs.acs.org/10.1021/jacs.4c08097

Notes

The authors declare no competing financial interest.

ACKNOWLEDGMENTS

AMW would like to thank Dr. Michael D. Roy for assistance with and insights into EPR measurements of Co(II) complexes. We thank the US National Science Foundation for supporting this work via CHE-2246913. The purchase of the Bruker ULTRAFLEX III in 2008 was partially funded by the NIH NCRR 1S10RR024601-01 Award to the Department of Chemistry. The Bruker Quazar APEXII diffractometer was supported by a generous gift from Paul J. and Margaret M. Bender. The Bruker EleXsys E500 EPR spectrometer was supported by NSF CHE-0741901. The Quantum Design MPMS3 SQUID magnetometer with an EverCool System was additionally supported by the UW-Madison Department of Chemistry. The Bruker Advance Neo 500 spectrometer was supported by NSF CHE-2017891.

REFERENCES

(1) Amin, N.; Said, S.; Salleh, M.; Afifi, A.; Ibrahim, N.; Hasnan, M.; Tahir, M.; Hashim, N. Review of Fe-based spin crossover metal complexes in multiscale device architectures. *Inorg. Chim. Acta* **2023**, *544*, No. 121168.

(2) Wang, M.; Li, Z.-Y.; Ishikawa, R.; Yamashita, M. Spin crossover and valence tautomerism conductors. *Coor. Chem. Rev.* **2021**, *435*, 213819−213837.

(3) Gütlich, P.; Goodwin, H. A. *Spin crossover in transition metal compounds I*; Springer Science & Business Media, 2004; vol *1*.

(4) Gütlich, P.; Goodwin, H. A. *Spin crossover in transition metal compounds II*; Springer Science & Business Media: Heidelberg, 2004; vol *1*.

(5) Gütlich, P.; Goodwin, H. A. *Spin Crossover in Transition Metal Compounds III*; Springer Science & Business Media, 2004; vol *1*.

(6) Guionneau, P.; Marchivie, M.; Bravic, G.; Letard, J.; Chasseau, D. Structural Aspects of Spin Crossover. Example of the (Fe^{II}Ln-$(NCS)_2$) Complexes. *Top. Curr. Chem.* **2004**, *234*, 97−128.

(7) Winkler, J. R.; Gray, H. B. Electronic Structures of Oxo-Metal Ions. In *Molecular Electronic Structures of Transition Metal Complexes I*; Mingos, D. M. P.; Day, P.; Dahl, J. P., Eds.; Springer Berlin Heidelberg: Berlin, 2012; pp 17−28.

(8) Koudriavtsev, A.; Linert, W. Spin crossover—An unusual chemical equilibrium. *J. Struct. Chem.* **2010**, *51*, 335−365.

(9) Gütlich, P.; Hauser, A.; Spiering, H. Thermal and optical switching of iron (II) complexes. *Angew. Chem., Int. Ed. Engl.* **1994**, *33* (20), 2024−2054.

(10) Zaz, M. Z.; Ekanayaka, T. K.; Cheng, R.; Dowben, P. A. Variability of the Conductance Changes Associated with the Change in the Spin State in Molecular Spin Crossover Complexes. *Magnetochemistry* **2023**, *9* (11), 223.

(11) Carney, M.; Papaefthymiou, G.; Spartalian, K.; Frankel, R.; Holm, R. H. Ground spin state variability in $[Fe_4S_4(SR)_4]^{3-}$: Synthetic analogs of the reduced clusters in ferredoxins and other iron-sulfur proteins: cases of extreme sensitivity of electronic state and structure to extrinsic factors. *J. Am. Chem. Soc.* **1988**, *110* (18), 6084−6095.

(12) Infante, I.; Andrews, L.; Wang, X.; Gagliardi, L. Noble gas matrices may change the electronic structure of trapped molecules: the $UO_2(Ng)_4$ [Ng = Ne, Ar] case. *Chem.—Eur. J.* **2010**, *16*, 12804−12807.

(13) Liang, B.; Andrews, L.; Li, J.; Bursten, B. E. Noble Gas−Actinide Compounds: Evidence for the Formation of Distinct $CUO(Ar)_{4-n}(Xe)_n$ and $CUO(Ar)_{4-n}(Kr)_n$ (n = 1, 2, 3, 4) Complexes. *J. Am. Chem. Soc.* **2002**, *124* (31), 9016−9017.

(14) Clérac, R.; Cotton, F. A.; Daniels, L. M.; Dunbar, K. R.; Kirschbaum, K.; Murillo, C. A.; Pinkerton, A. A.; Schultz, A. J.; Wang, X. Linear tricobalt compounds with di(2-pyridyl)amide (dpa) ligands: Temperature dependence of the structural and magnetic properties of symmetrical and unsymmetrical forms of $Co_3(dpa)_4Cl_2$ in the solid state. *J. Am. Chem. Soc.* **2000**, *122* (26), 6226−6236.

(15) Pantazis, D. A.; McGrady, J. E. A three-state model for the polymorphism in linear tricobalt compounds. *J. Am. Chem. Soc.* **2006**, *128* (12), 4128−4135.

(16) Milocco, F.; de Vries, F.; Siebe, H. S.; Engbers, S.; Demeshko, S.; Meyer, F.; Otten, E. Widening the Window of Spin-Crossover Temperatures in Bis(formazanate)iron(II) Complexes via Steric and Noncovalent Interactions. *Inorg. Chem.* **2021**, *60* (3), 2045−2055.

(17) Ouyang, Z.; Meng, Y.; Cheng, J.; Xiao, J.; Gao, S.; Deng, L. Three- and Four-Coordinate Homoleptic Iron(I)−NHC Complexes: Synthesis and Characterization. *Organometallics* **2016**, *35* (10), 1361−1367.

(18) Liu, Y. Z.; Wang, J.; Zhao, Y.; Chen, L.; Chen, X. T.; Xue, Z. L. Four-coordinate Co(II) and Fe(II) complexes with bis(N-heterocyclic carbene)borate and their magnetic properties. *Dalton Trans* **2015**, *44* (3), 908−911.

(19) Cibian, M.; Hanan, G. S. Geometry and Spin Change at the Heart of a Cobalt(II) Complex: A Special Case of Solvatomorphism. *Chemistry* **2015**, *21* (26), 9474−9481.

(20) Wolny, J. A.; Rudolf, M. F.; Ciunik, Z.; Gatner, K.; Wołowiec, S. Cobalt (II) triazene 1-oxide bis(chelates). A case of planar (low spin)−tetrahedral (high spin) isomerism. *J. Chem. Soc., Dalton Trans.* **1993**, *10*, 1611−1622.

(21) Matouzenko, G. S.; Bousseksou, A.; Lecocq, S.; van Koningsbruggen, P. J.; Perrin, M.; Kahn, O.; Collet, A. Polymorphism in spin transition systems. Crystal structure, magnetic properties, and mössbauer spectroscopy of three polymorphic modifications of $[Fe(dppa)(NCS)_2]$ [dppa = (3-aminopropyl)bis(2-pyridylmethyl)-amine]. *Inorg. Chem.* **1997**, *36* (25), 5869−5879.

(22) Zein, S.; Matouzenko, G. S.; Borshch, S. A. Quantum chemical study of three polymorphs of the mononuclear spin-transition complex $[Fe(DPPA)(NCS)_2]$. *J. Phys. Chem. A* **2005**, *109* (38), 8568−8571.

(23) Haryono, M.; Heinemann, F. W.; Petukhov, K.; Gieb, K.; Müller, P.; Grohmann, A. Parallel Crystallization of a "Static" and a Spin-Crossover Polymorph of an Iron(II) Complex from the Same Solution. *Eur. J. Inorg. Chem.* **2009**, *2009* (14), 2136−2143.

(24) Halcrow, M. A. Structure:Function Relationships in Molecular Spin-Crossover Materials. *In Spin-Crossover Materials* **2013**, 147−169.
(25) Shaffer, D. W.; Bhowmick, I.; Rheingold, A. L.; Tsay, C.; Livesay, B. N.; Shores, M. P.; Yang, J. Y. Spin-state diversity in a series of Co(II) PNP pincer bromide complexes. *Dalton Trans* **2016**, *45* (44), 17910−17917.
(26) Nippe, M.; Victor, E.; Berry, J. F. Do Metal-Metal Multiply-Bonded "Ligands" Have a trans Influence? Structural and Magnetic Comparisons of Heterometallic Cr≡Cr···Co and Mo≡Mo···Co Interactions. *Eur. J. Inorg. Chem.* **2008**, *2008* (36), 5569−5572.
(27) Chipman, J. A.; Berry, J. F. Paramagnetic Metal-Metal Bonded Heterometallic Complexes. *Chem. Rev.* **2020**, *120* (5), 2409−2447.
(28) Wheaton, A. M.; Chipman, J. A.; Roy, M. D.; Berry, J. F. Metal-Metal Bond Umpolung in Heterometallic Extended Metal Atom Chains. *Inorg. Chem.* **2022**, *61*, 15058−15069.
(29) Pyykkö, P.; Atsumi, M. Molecular single-bond covalent radii for elements 1−118. *Chemistry* **2009**, *15* (1), 186−197.
(30) Alvarez, S. A cartography of the van der Waals territories. *Dalton Trans.* **2013**, *42* (24), 8617−8636.
(31) Clérac, R.; Cotton, F. A.; Daniels, L. M.; Dunbar, K. R.; Murillo, C. A.; Wang, X. Structural and magnetic properties of $Co_3(dpa)_4Br_2$. *J. Chem. Soc., Dalton Trans.* **2001**, *4*, 386−391.
(32) Clérac, R.; Cotton, F. A.; Daniels, L. M.; Dunbar, K. R.; Murillo, C. A.; Wang, X. Tuning the Metal−Metal Bonds in the Linear Tricobalt Compound $Co_3(dpa)_4Cl_2$: Bond-Stretch and Spin-State Isomers. *Inorg. Chem.* **2001**, *40* (6), 1256−1264.
(33) Clérac, R.; Cotton, F. A.; Jeffery, S. P.; Murillo, C. A.; Wang, X. Compounds with symmetrical tricobalt chains wrapped by dipyridylamide ligands and cyanide or isothiocyanate ions as terminal ligands. *Inorg. Chem.* **2001**, *40* (6), 1265−1270.
(34) Srinivasan, A.; Wang, X.; Clérac, R.; Rouzieres, M.; Falvello, L. R.; McGrady, J. E.; Hillard, E. A. Temperature dependence of the spin state and geometry in tricobalt paddlewheel complexes with halide axial ligands. *Dalton Trans.* **2018**, *47* (46), 16798−16806.
(35) Kahn, O. *Molecular magnetism*; Wiley-VCH: New York, 1993.
(36) Thomas-Colwell, J.; Sookezian, A.; Kurtz, D. A.; Kallick, J.; Henling, L. M.; Stich, T. A.; Hill, M. G.; Hunter, B. M. Tuning Cobalt(II) Phosphine Complexes to be Axially Ambivalent. *Inorg. Chem.* **2022**, *61* (32), 12625−12634.
(37) Ekanayaka, T. K.; Maity, K. P.; Doudin, B.; Dowben, P. A. Dynamics of spin crossover molecular complexes. *Nanomaterials* **2022**, *12* (10), 1742.
(38) Rohmer, M.-M.; Strich, A.; Bénard, M.; Malrieu, J.-P. Metal−Metal Bond Length Variability in $Co_3(dipyridylamide)_4Cl_2$: Bond-Stretch Isomerism, Crystal Field Effects, or Spin Transition Process? A DFT Study. *J. Am. Chem. Soc.* **2001**, *123* (37), 9126−9134.
(39) Lehr, M.; Paschelke, T.; Trumpf, E.; Vogt, A. M.; Nather, C.; Sonnichsen, F. D.; McConnell, A. J. A Paramagnetic NMR Spectroscopy Toolbox for the Characterisation of Paramagnetic/Spin-Crossover Coordination Complexes and Metal-Organic Cages. *Angew. Chem., Int. Ed. Engl.* **2020**, *59* (43), 19344−19351.

https://doi.org/10.1021/jacs.4c08097
J. Am. Chem. Soc. 2024, 146, 26926−26935